Ab initio study of γ-Al_2O_3 surfaces

Henry P. Pinto,[1,*] R. M. Nieminen,[2,†] and Simon D. Elliott[1,‡]
[1]*NMRC, University College Cork, Lee Maltings, Prospect Row, Cork, Ireland*
[2]*Laboratory of Physics, Helsinki University of Technology, P.O. Box 1100, FIN-02015 HUT, Espoo, Finland*
(Received 16 December 2003; revised manuscript received 6 April 2004; published 3 September 2004)

Starting from the theoretical prediction of the γ-Al_2O_3 structure using density-functional theory in the generalized gradient approximation, we have studied the (1 1 1), (0 0 1), (1 1 0), and (1 5 0) surfaces. The surface energies and their corresponding structures are computed and compared with predictions for (0 0 0 1) α-Al_2O_3 and available experimental results for γ-alumina surfaces. (1 1 1) and (0 0 1) surfaces are predicted to be equally stable, but to show quite different structure and reactivity. Whereas a low coverage of highly reactive trigonal Al occurs on (1 1 1), (0 0 1) exhibits a more dense plane of both five-coordinate and tetrahedral Al. Microfaceting of a (1 1 0) surface into (1 1 1)-like planes is also observed. The implications for the structure of ultrathin dielectric films and for the surfaces of disordered transition aluminas are discussed.

DOI: 10.1103/PhysRevB.70.125402 PACS number(s): 68.47.Gh, 68.35.Bs, 73.20.−r, 71.15.Mb

I. INTRODUCTION

Considering the technological importance of alumina (Al_2O_3), it is surprising that no reliable atomic-scale model exists for the surface structure of the amorphous phase or of the transition aluminas. This is partly due to experimental difficulties in preparing uniform surfaces, free of impurities, but also due to the structural complexity of the bulk phases and the need for high-quality theoretical treatments.[1] Developing and understanding structural models for the surfaces of the transition alumina γ-Al_2O_3 is the aim of this work.

Alumina is a widely used ceramic and many applications depend on its surface properties, e.g., as ultra-hard coatings, microporous catalysts, and in electroluminescent flat-screen displays.[2] As a modestly high-permittivity material with a large band gap and abrupt interface to Si, thin-film Al_2O_3 is already being used in read/write heads[3] and node dynamic random access memory (DRAM)[4] and is a candidate gate dielectric for next-generation transistors.[5] Integration into these technologies places stringent demands on processing and performance of the active thin film, and so requires an understanding of the film surface.

Alumina can be prepared in a variety of solid polymorphs. Corundum or sapphire, α-Al_2O_3, is the most stable. Its bulk structure may be described as a hcp O sublattice with two-thirds of the octahedral interstices filled by Al (see Sec. III). Surfaces of α-Al_2O_3 have been well studied, especially the (0 0 0 1) basal plane.[6–10] We therefore validate our method on this system. Bauxite ore, the source of aluminium and alumina, is purified by conversion to an aluminium hydroxide and subsequent dehydration. This yields α-Al_2O_3 via the series of metastable "transition alumina" phases.[1,11] For instance, dehydrating boehmite γ-AlOOH at 300–500 °C gives γ-Al_2O_3, then δ-Al2O3 (700–800 °C), θ-Al_2O_3 (900–1000 °C), and finally α-Al_2O_3 (1000–1100 °C). The α-Al_2O_3, δ, and θ transition aluminas are all based on an hcp O sublattice but differ in the distribution of four- and six-coordinate Al cations: γ and δ are spinel like (as is η, a dehydration product of bayerite). Clearly, bulk thermodynamics alone cannot explain the occurrence of these distinct spinel-based phases; rather, they result from the kinetics of dehydration and ionic diffusion specific to each preparation process.[11–13]

Our computational study is intended to predict the surface structure of spinel-based transition aluminas, such as δ- and γ-Al_2O_3, when fully dehydroxylated. These are compared to a similar surface of α-Al_2O_3. Bare surfaces are the subject of this paper, but recognizing the ubiquity and importance of hydrogen at alumina surfaces, our later work will consider hydroxylation. Our ultimate interest is in the surface of amorphous films, where O is also likely to be approximately close packed and where Al is distributed between four- and six-coordinated sites.[14,17] Alumina is a *p*-block metal oxide with a wide bad gap (ca. 9 eV) and it does not readily form suboxides (ratio $Al:O < 2:3$). The occurrence of O vacancies is not fully understood:[15] in a recent theoretical study on both bulk and (0 0 0 1) α-Al_2O_3,[16] the authors have computed O-vacancy formation energies of the order of 10 eV both in the bulk and at the surface. On the other hand, experimental results show that annealing of alumina in ultra-high vacuum yields metallic Al overlayers rather than a suboxide.[18] In any case, we are interested in gamma-alumina samples that have been prepared under oxygen-rich conditions, e.g., by dehydration of hydroxide or by chemical vapor deposition. In the latter case, alumina films of stoichiometry $Al:O = 2:3$ are deposited, even for 1 nm films on HF-treated Si.[5] We therefore restrict our study to such stoichiometric slabs/surfaces.

Much recent experimental and theoretical work has addressed the controversial question of the bulk structure of γ-Al_2O_3, as summarized in Refs. 11 and 19. γ-Al_2O_3 is a defective spinel and so the main point of contention is the cation vacancy distribution. In a hypothetical Al_3O_4 spinel, two-thirds of Al are octahedrally coordinated to O (O_h) and one-third tetrahedral (T_d), the latter in pairs that face-share vacant Al octahedra (V_{O_h}). More cation vacancies (V_{O_h} or V_{T_d}) must therefore be introduced into this spinel to reduce the Al concentration by one-ninth and produce the sesquioxide stoichiometry. Of the N octahedral and $2N$ tetrahedral interstices of the fcc sublattice of N oxide anions, only $2N/3$

should be occupied by Al cations and this can be achieved in about 10^{10} distinct ways.[12] Most authors agree that V_{O_h} are favored,[11,19,20] but that there is a statistical distribution of up to 30% V_{T_d} in a room-temperature sample of γ-Al_2O_3.[21,22]

Much of the catalytic activity of alumina surfaces can be traced to the electronic structure. Coordinatively unsaturated Al ions at the surface show empty surface states, typically within the bulk band gap and localized primarily on Al. The closer these states lie to the Fermi level, the more reactive these sites are towards electron-rich adsorbates, i.e., the higher their Lewis acidity. Beyond this, however, consensus is lacking. A Fourier transform-infrared (FT-IR) study of partially dehydroxylated γ-Al_2O_3 with adsorbed pyridine shows three types of Lewis acid site on the surface, assigned to three-, four-, and five-coordinate Al.[23] On the other hand, solid-state NMR indicates a variety of surface Al, none of which can be assigned as three coordinate (trigonal).[24]

Considering theoretical approaches to modeling alumina, rigid pair potentials are found to be inadequate for the bulk, requiring charge transfer[12] or quadrupolar corrections.[25] Studies using the more reliable but computationally demanding density-functional theory (DFT) have concentrated on the (0 0 1) and (1 1 0) surfaces of γ-Al_2O_3, in implementations that model the surface as a periodic slab[26–28] or as a cluster.[29] However, some of these suffer from deficiencies in modeling γ-Al_2O_3 (nonstoichiometry, absence of vacancies or high H concentration) or in adequately representing a surface (insufficient slab area or thickness, frozen atoms). More relevant for the current work on close-packed O surfaces is a periodic DFT study of the hcp-based κ-Al_2O_3 and its close-packed (0 0 1)-like surfaces:[30] significant relaxation of surface Al is discussed in terms of subsurface tetrahedral Al and vacancies.

II. COMPUTATIONAL METHOD

First-principles calculations give a reliable description of materials and their surfaces at the atomic scale and we apply this method to alumina using the VASP code.[31,32] In order to compute the ground-state electronic wave function within periodic boundary conditions, a plane-wave (PW) basis set and Vanderbilt ultrasoft pseudopotentials (USPP)[33,34] are used. Electron correlation is accounted for in an approximate way by use of DFT in the generalized gradient approximation (GGA) as parametrized by Perdew and Wang (GGA-II or PW91).[35]

In order to obtain self-consistent valence-electron wave functions by minimizing the Kohn-Sham total energy functional, we use the residual minimization scheme (RMM-DIIS).[34] Convergence with respect to k points of less than 0.02 eV/Al_2O_3 is achieved with a suitable Monkhorst-Pack mesh[36] and a PW kinetic energy cutoff of 396 eV. A Fermi-level smearing of 0.1 eV is used for improving the total-energy convergence. Finally, the ions are allowed to relax until the forces are less than 0.03 eV/Å. In order to compare our results we perform several computations using the CASTEP code[37] within the GGA-II approach and Vanderbilt USPP with a $(4\times4\times1)$ Monkhorst-Pack mesh and a kinetic cutoff energy of 390 eV; within these parameters we converge the total energy to less than 0.02 eV/Al_2O_3. The ionic relaxation is performed until the root-mean-square forces are less than 0.03 eV/Å. It is important to stress the fact that we use GGA-generated USPP within VASP computations while in CASTEP we use local-density approximation (LDA)-generated USPP. It is worthwhile mentioning that although LDA and GGA yield similar results, GGA is better in describing the structure and energetics of alumina polymorphs.[11]

In order to get a more fundamental understanding about the bonding in both bulk and surfaces of γ-Al_2O_3, Mulliken population analysis[38] has been performed. It is well known that the PW basis set is deficient in quantifying local atomic properties. We have therefore used the technique suggested by Sánchez-Portal *et al.*[39,40] for projecting the PW onto a basis that is a linear combination of atomic orbitals (LCAO). The quality of this technique is measured by the so-called spilling parameter that in our case is less than 0.008.

Finally, in order to check the robustness of selected surfaces, we performed microcanonical molecular dynamics (MD) using VASP. The total free energy is conserved and the velocity-Verlet algorithm for integrating the Newton's equations is used. Throughout these simulations, we allow electronic relaxation in order to keep the electrons near the Born-Oppenheimer surface. The ionic time step was 2 fs and the whole simulations lasted 0.3 ps at an approximated temperature of 700 K, appropriate for the conversion of hydroxides to γ- or η-Al_2O_3 (500–800 K) and much lower than that required to form θ- or α-Al_2O_3 (1100 K, 1300 K).[13] The supercell is held fixed throughout the MD run, which also prevents any unwanted decomposition of bulk γ-Al_2O_3 within the slab. We note that the computed mean square displacements (MSD) values are only a coarse approximation, due to the short MD time carried out.

III. STRUCTURAL AND ELECTRONIC PROPERTIES OF BULK γ-Al_2O_3

To validate our method and serve as a reference, we computed bulk corundum, α-Al_2O_3. The hexagonal unit cell contains 30 ions, arranged in six (0 0 0 1) Al_2O_3 layers. Al cations in local D_{3d} symmetry occupy two-thirds of the octahedral sites between alternating layers of hcp O anions. The geometry of both cell and ions was optimized as detailed above to yield $a=4.751$ Å, $c/a=2.757$, which agrees with experiment ($a=4.751$ Å, $c/a=2.730$)[1] within the accuracy expected for GGA. This corresponds to a [0 0 0 1] spacing of 2.18 Å between O layers.

As mentioned in the introduction, γ-Al_2O_3 has a defective spinel structure and the smallest stoichiometric cell is built up by stacking three $MgAl_2O_4$ primitive cells (space group $Fd\bar{3}m$), replacing all the Mg with Al and finally extracting two Al atoms to give vacancies. Since this aluminium sublattice possesses 6 T_d and 12 O_h sites per cell, there are then 17 possible nonequivalent configurations for locating 16 atoms on these sites. Of these, four have two Al vacancies on T_d sites (T_dT_d), five show both vacancies on O_h sites (O_hO_h), and eight are mixed (O_hT_d).

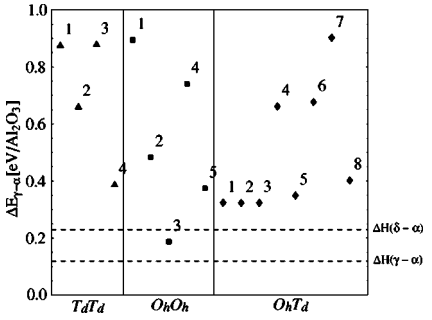

FIG. 1. Calculated relative energies per unit formula after full relaxation for the 17 nonequivalent structures for bulk γ-Al_2O_3 with respect to the α-Al_2O_3. The horizontal dashed lines labeled as $\Delta H(\gamma\text{-}\alpha)$ and $\Delta H(\delta\text{-}\alpha)$ represent the experimental transformation enthalpies of gamma and delta aluminas with respect to alpha alumina,[41] respectively.

Having recognized those structures, a full relaxation of cell shape, volume, and atoms was carried out on each of the 17 structures using a $(2\times2\times2)$ *k*-point mesh (including the Γ point. The outcome of these relaxations is pictured in Fig. 1; as expected for a nonisotropic distribution of vacancies, the optimized primitive cells do not correspond to cubic cells, and so reflect the local asymmetry of the various vacancy distributions. From the results, the lowest energy structure is the $O_hO_h(3)$ system with the maximum spacing between O_h vacancies ($\sim$7.45 Å within the cell) in agreement with other DFT studies.[11,14] This is the model which we use for γ-Al_2O_3. As shown in Fig. 1, the bulk energy is 0.18 eV/Al_2O_3 higher than that computed for α-Al_2O_3. Less stable by 0.14 eV/Al_2O_3 are three structures with mixed vacancy sites O_hT_d, isoenergetic at this level of computational precision (0.02 eV/Al_2O_3). A full relaxation of the $O_hO_h(3)$ and $O_hT_d(2)$ systems using the CASTEP code yields the same difference in energies (0.143 eV/Al_2O_3). It is interesting to compare our results with a previous work using LDA[14] within a cubic cell: the same structures are found to be lowest in energy but with an energy difference of 0.16 eV/Al_2O_3.

In Table I and Fig. 2 we present the structure of the proposed bulk γ-Al_2O_3. The $C2/m$ space group of this structure points out its deviation from cubic spinel when γ-alumina is viewed locally. Reoccupying the vacancies allowed us to fit the structure to cubic symmetry (0.35 Å tolerance), yielding a cell parameter $a=7.99$ Å. The average spacing between O layers is 2.29 Å (along [1 1 1] in the cubic spinel). In the literature one can find a scatter with respect to the experimental value of *a* (in cubic symmetry) from 7.911–7.943 Å.[13,21] Thus, our result is $\sim$1% greater than the experimental values and in close agreement with other GGA results.[27] It is well known that, in general, GGA overestimates lattice parameters. The deviation from cubic symmetry reflects the noncubic ordering of gamma alumina in agreement with the measured x-ray diffraction (XRD) powder patterns in this compound.[13] We suggest that our locally noncubic model should give good predictions for real gamma alumina since the properties of materials with a certain degree of disorder are governed by local structure. The calculated bulk modulus for γ-Al_2O_3 is 209 GPa, in good agreement with the LDA value of 219 GPa obtained in a previous work.[14] For comparison, the lattice parameter predicted using CASTEP is 7.797 Å. This last result reflects the importance of internally consistent calculations using GGA-generated USPP (see Sec. II). Finally it is useful to point out that the two Al vacancies are nonequivalent and their fractional coordinates are $(1/2,1/2,0)$ and $(0,0,1/2)$ in the primitive cell with $C2/m$ symmetry as shown in Fig. 2.

TABLE I. Crystallographic data for computed γ-Al_2O_3 after finding the symmetry with a tolerance of 0.01 Å from the $O_hO_h(3)$ model. Al_{T_d} and Al_{O_h} represent the Al atoms in tetrahedral and octahedral sites, respectively, while u,v,w are the fractional coordinates. The atom labels correspond with Fig. 2.

Property	Calculated (GGA)		
Space group	$C2/m$		
$a=b$(Å)	5.663		
c/a	2.421		
$\alpha=\beta$(°)	90.6		
γ(°)	60.401		
Volume (Å^3)	382.326		
B_o(GPa)	209		
Sites	u	v	w
$Al(1)_{T_d}$	0.0039	0.0039	0.1225
$Al(2)_{T_d}$	0.3247	0.3247	0.2070
$Al(3)_{T_d}$	0.6658	0.6658	0.5482
$Al(4)_{O_h}$	0	0.5	0
$Al(5)_{O_h}$	0.6511	0.6511	0.1603
$Al(6)_{O_h}$	0.1650	0.1650	0.6603
$Al(7)_{O_h}$	0.6756	0.1639	0.6593
O(1)	0.8452	0.3456	0.0866
O(2)	0.8346	0.3320	0.5935
O(3)	0.4887	0.0308	0.7452
O(4)	0.8240	0.8240	0.0834
O(5)	0.6791	0.6791	0.9202
O(6)	0.8344	0.8344	0.5934
O(7)	0.4943	0.4943	0.7476
O(8)	0.0026	0.0026	0.7416
O(9)	0.3351	0.3351	0.5865
V_{1O_h}	0	0	0.5
V_{2O_h}	0.5	0.5	0

In addition, we have calculated the partial density of states (PDOS) for the proposed bulk structure $[O_hO_h(3)]$ as well as its total DOS and the band structure (Fig. 3 and Fig. 4). The first clear feature from Fig. 3 is that almost all the valence charge is associated with oxygen atoms, suggesting a highly polar character of the Al-O bonding, consistent with previous works on κ-Al_2O_3 and α-Al_2O_3.[42,43] In fact, the lower and upper valence bands are dominated by O-*s* and O-*p*, respectively, with a small contribution from Al-*s*, -*p*, and -*d* in each.

In Fig. 4 the electronic band structure of $O_hO_h(3)$ shows a direct band gap of 3.97 eV at the Γ point in contrast to the

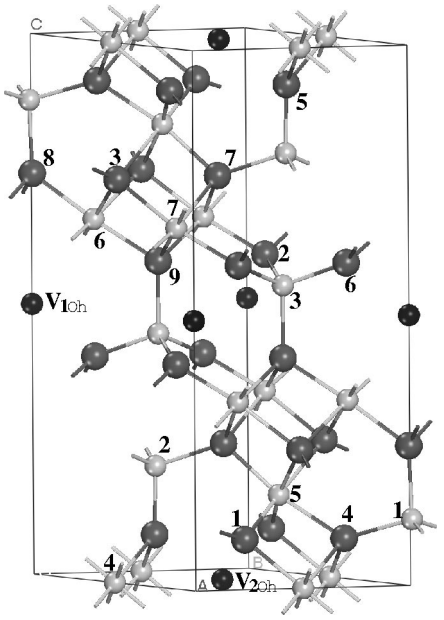

FIG. 2. Predicted crystal structure for γ-Al_2O_3 with $C2/m$ space group [$O_hO_h(3)$ model]. Here the [0 0 1] direction coincides with the [1 1 1] direction in the cubic spinel structure. In the figure, the white, gray, and black spheres represent Al, O, and V_{O_h}, respectively.

experimental value of 8.5 eV (Ref. 44) — a deficiency typical of DFT methods. Nevertheless, the predicted value is in excellent agreement with that obtained using LDA.[14] The flatness of the bands in the top of the upper valence band (UVB), especially along the A-Γ-Z points, denotes the tightly localized bonding of the corresponding electrons to the host atoms. Besides, we also observed that these topmost bands are noticeably separate from the rest of the UVB. This special feature is related with the fact that γ-Al_2O_3 has a layered-like structure. As illustrated in Fig. 5, the electronic distribution of the highest UVB band in the energy range of 0–0.01 eV below the band gap shows high electronic localization on the O atoms nearest to the vacancy sites.

The Mulliken population analysis results for the $O_hO_h(3)$ model of γ-Al_2O_3 is presented in Table II. For comparative purposes, we have carried out the same analysis on α-Al_2O_3 as well. As mentioned in the previous section, the spilling parameter[39,40] ranged between 0.008 and 0.007, indicating a reliable projection to the LCAO basis set. In the α-Al_2O_3 crystal, the Al-O overlap populations n_m(Al-O) are 0.34 and 0.27 e (mean=0.31 e) with bond lengths of 1.868 and 1.993 Å, respectively, with a mean of 1.924 Å. The effective ionic valence charge (q_{eff}) is 1.38 e. These values, especially the overlap population n_m, measure the crystal ionicity: a higher value of n_m means a higher degree of covalency in the bond. The results suggest that α-alumina shows predominantly ionic bonding with a small level of covalency. The results for γ-Al_2O_3 are more involved due to the small deviation from the perfect spinel structure. A close inspection shows that the Al_{T_d}-O bonding is more covalent

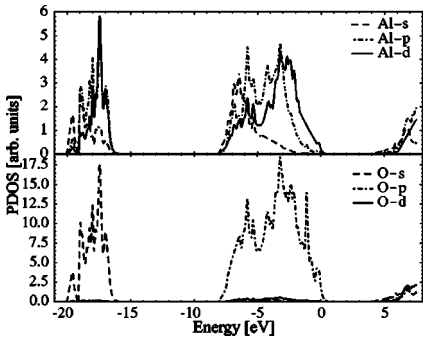

FIG. 3. Calculated PDOS of γ-Al_2O_3, the Fermi level is aligned to 0 on the x axis. Note the differing y axis scales.

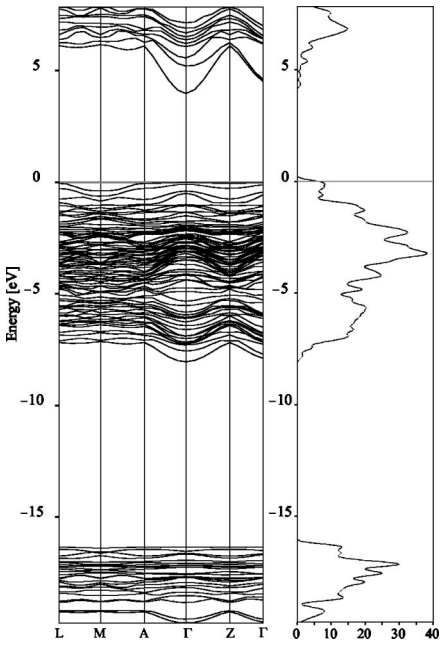

FIG. 4. Computed electronic band structure and total density of states for γ-Al_2O_3.

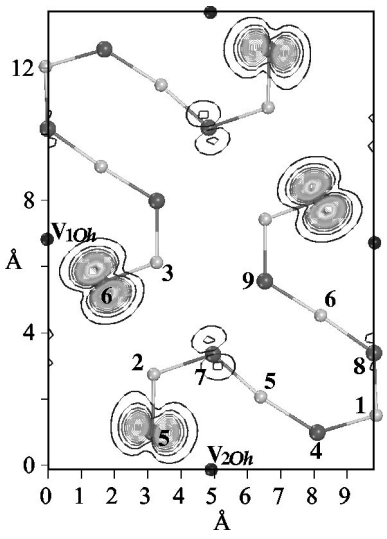

FIG. 5. Electronic density of the top band in the UVB for γ-Al_2O_3. The gray, white, and black spheres represent the O, Al, and vacancy sites, respectively. The numeration is according to Table I and Fig. 2.

TABLE II. Mulliken population analysis for α-Al_2O_3 and γ-Al_2O_3. The averaged effective ionic charge ($\overline{q}_{\text{eff}}$) and overlap population ($\overline{n}_m$) are in *e* units while the averaged bonding distances ($\overline{d}$) are in Å.

	$\overline{q}_{\text{eff}}$(Al)	$\overline{n}_m$(Al-O)	$\overline{d}$(Al-O)
α-Al_2O_3:Al_{O_h}	1.38	0.31	1.92
γ-Al_2O_3:Al_{O_h}	1.39	0.33	1.94
γ-Al_2O_3:Al_{T_d}	1.28	0.49	1.81

than the Al_{O_h}-O. Comparison with the overlap population values for α-Al_2O_3 suggests to us that gamma is less ionic than alpha alumina.

IV. ENERGETICS AND STRUCTURAL PROPERTIES OF γ-Al_2O_3 SURFACES

A. Surface energies

Having resolved a likely structure for bulk γ-Al_2O_3, we proceed to investigate the (1 1 1), (0 0 1), (1 1 0), and (1 5 0) surfaces. The cleaving planes were chosen in such a way to cross the maximum amount of Al-vacancy sites. That is the reason why the rather high index (1 5 0) surface appears as a viable choice. In particular along {1 1 1} we consider two surfaces: cleaving through the V_{1O_h}-$Al(3)_{T_d}$ plane yields (1 1 1)*a*, while the V_{2O_h}-$Al(4)_{O_h}$ plane is denoted (1 1 1)*b* (Fig. 2). Note that [1 1 1], [0 0 1], and [1 5 0] in the cubic system are equivalent to [0 0 1], [1 1 0], and [1 1 1], respectively, in the cell displayed in Fig. 2. In order to minimize the dipole moment in the supercells, we built the slabs with similar surfaces in each side of the slab and kept Al_2O_3 stoichiometry throughout.

The *k*-point mesh depended on the slab under study: for (1 1 1), (0 0 1), (1 1 0), or (1 5 0) we used a *k*-point mesh including Γ of $(2\times2\times1)$, $(2\times4\times1)$, $(2\times3\times1)$, and $(4\times2\times1)$, respectively, in order to converge the slab total energy to <5 meV/atom. Furthermore, our tests show that a vacuum of 10 Å is adequate to eliminate the surface-surface artifact interaction. Using the standard method,[45] we subtract the surface energy per unit area (σ) of the slabs with the equation

$$\sigma = \frac{1}{A}\lim_{N\to\infty}\frac{1}{2}(E^N_{\text{slab}} - NE_{\text{bulk}}), \tag{1}$$

where A is the slab area, E^N_{slab} is the total energy of the N-atom slab, and E_{bulk} is the bulk total energy. Here the limit is approximated with the Nth term. However, rather than use E_{bulk} from the calculations of Sec. III, we use the more consistent value given by the slope of the linear polynomial fitted to E^N_{slab} versus N, as suggested in previous works.[46,47] When the convergence is reached there is a linear dependence of E^N_{slab} with respect to N,

$$E^N_{\text{slab}} \approx 2A\sigma + NE_{\text{bulk}}. \tag{2}$$

So, the slope is the bulk energy, which is then replaced in Eq. (1) to yield the surface energy. We calculated the energy of several slabs with different thicknesses, keeping Al_2O_3 stoichiometry throughout. In order to obtain an accurate interpolation in Eq. (2) for E_{bulk} and then to obtain σ, we carried out full relaxations on the internal coordinates of slabs containing 40, 80, and 120 atoms for the (1 1 1) slabs; for the (0 0 1), (1 1 0), and (1 5 0) slabs we used 80 and 100 atoms. We observed metallic behavior in some of the unrelaxed slabs, but on complete optimization of the ions, the ground state becomes insulating. We would like to stress the fact that the computed surface energies are convergent values that have become independent of the number of atoms [N in Eqs. (1) and (2)].

TABLE III. Calculated α-Al_2O_3 (0001) and γ-Al_2O_3 surface energies for relaxed (σ_R) and static (σ_S) slabs.

Surface	Slab size (atoms)	σ_R(J/m^2)	σ_S(J/m^2)
α-(0 0 0 1)	60	1.54	3.15
γ-(1 1 1)*a*	40	0.95	1.62
γ-(1 1 1)*b*	40	1.85	3.57
γ−(0 0 1)	100	1.05	2.97
γ-(1 1 0)	100	1.53	3.43
γ-(1 5 0)	80	1.91	2.79

Considering convergence with respect to slab thickness, we found that for the (1 1 1)*a* and *b* surfaces, 40-atom (eight layer) slabs were adequate to converge the surface energy to <0.07 J/m^2, while for the others, 80- or 100-atom slabs were needed in order to keep the same convergence. From our calculations, (1 1 1)*a* is the most stable surface with $\sigma_R = 0.95$ J/m^2 and its enhanced stability is discussed below; the next stable surface is (0 0 1) with $\sigma_R = 1.05$ J/m^2 (see Table III). Following the same method for estimating the surface energy using CASTEP, the (1 1 1)*a* energy is 1.04 J/m^2 in good accordance with the VASP predicted value.

It is useful to compare our γ-(1 1 1) surfaces with the well-characterized (0 0 0 1) basal plane of α-Al_2O_3, since this also shows close-packed O layers. Using our model for bulk α (Sec. III) and following published work[1,6,48–50] we generated a slab model for the Al-terminated (0 0 0 1) surface. Convergence of σ to <0.05 J/m^2 was achieved with respect to slab thickness (six layers, 13.1 Å), vacuum thickness (13.1 Å) and *k*-point mesh $(2\times2\times1)$ including Γ. Interpolation across $\leqslant$60-atom slabs yields $\sigma_R = 1.54$ J/m^2.

The total energy of a solid sample is the sum of bulk and surface contributions. Since γ-alumina shows a lower surface energy than α-alumina, but higher bulk energy, there must exist some critical molar surface area A at which the two polymorphs show the same total energy and are in thermodynamic equilibrium. Using our calculated values of $\Delta\sigma(\alpha-\gamma) = +0.59$ J/m^2 and $\Delta E_{\text{bulk}}(\alpha-\gamma) = -0.178$ eV/Al_2O_3 $= -17.2$ kJ/mol yields a critical A of about 29 000 m^2/mol or 290 ± 10 m^2/g (the latter obtained using the molar mass of 102 g/mol). A lower value, $A = 125$ m^2/g, is reported from high-temperature calorimetry of hydrated aluminas,[48] in agreement with molecular dynamics simulations.[50] Commercial samples of γ-Al_2O_3 show surface areas ranging from 75–250 m^2/g.[23,24,48] Our calcula-

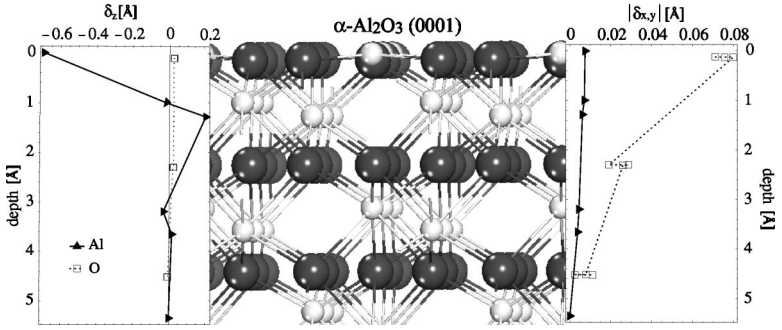

FIG. 6. Ionic displacements for the (0 0 0 1) α-alumina as a function of depth within the slab. The positive (negative) values of δ_z mean outward (inward) displacement fo the layers with respect to the middle of the slab. The filled triangles and the boxes represent the Al and O layers, respectively. The marks are joined for ease of visualization.

tions indicate that alumina of slightly higher porosity, with an internal surface area $>300\ m^2/g$, would be thermodynamically stable as the γ polymorph.

With growing interest in ultrathin films of alumina for electronics applications, we note that films <9 Å thick also show surface areas of $>300\ m^2/g$. This estimate assumes an averaged density of $3.8\ g/cm^3$ and neglects interfacial interactions, which may in fact dominate in such a thin film. Transition phases, such as γ-Al_2O_3, will therefore be thermodynamically favored during the early stages of film deposition (9 Å represents about four alumina layers). Thicker γ-Al_2O_3 films will be metastable, producing α-Al_2O_3 when annealed.

B. Surface structure

Starting from the bulk perfect sites we carried out a full ionic relaxation of the atoms in the slab until the forces were less than 0.03 eV/Å. Figures 6–8, 10, and 11 show the outcome of such relaxations plotted as a function of depth within the slab. In these figures, the projection of the marks onto the depth axis represents the final position of the oxygen and aluminium sublattice planes normal to the surface with respect to the most superficial atom, revealing how the Al and O layers are arranged. On the other hand, the x axis represents the ionic displacements normal (δ_z) and parallel ($|\delta_{x,y}|$) to the surface of the oxygen and aluminium atomic layers with respect to their perfect sites in the bulk.

In order to have a reference point, consolidate our method, and understand properly the ionic relaxations, we are going to analyze thoroughly the (0 0 0 1) α-alumina as presented in Fig. 6. Al and O layers are quite clear: $MO_3/M/M/O_3/M/M/O_3$. Trigonal symmetry constrains the surface O in [0 0 0 1] (δ_z displacements for O are negligible as shown in Fig. 6 left panel), so that the relaxation of the topmost Al into a near-trigonal site can only be accommodated by twisting within (0 0 0 1) ($|\delta_{x,y}|=0.07-0.08$ Å), as described in Ref. 8. The coverage of trigonal Al atop the close-packed O layer is $8.4\ \mu mol/m^2$.

From the left panel of Fig. 6 one can deduce the interlayer relaxations with respect to the corresponding bulk spacings. For instance, the topmost Al (depth=0 by definition) has an relaxation $\delta_z=-0.69$ Å, where the minus sign means that the movement was towards the bulk. Therefore, the original position of this Al was 0.69 Å above the surface. The first O layer at 0.12 Å deep, had an outward relaxation $\delta_z=0.03$ Å (i.e., the initial depth was 0.15 Å below the surface). From these data one can derive M-O_3 distances; the initial was

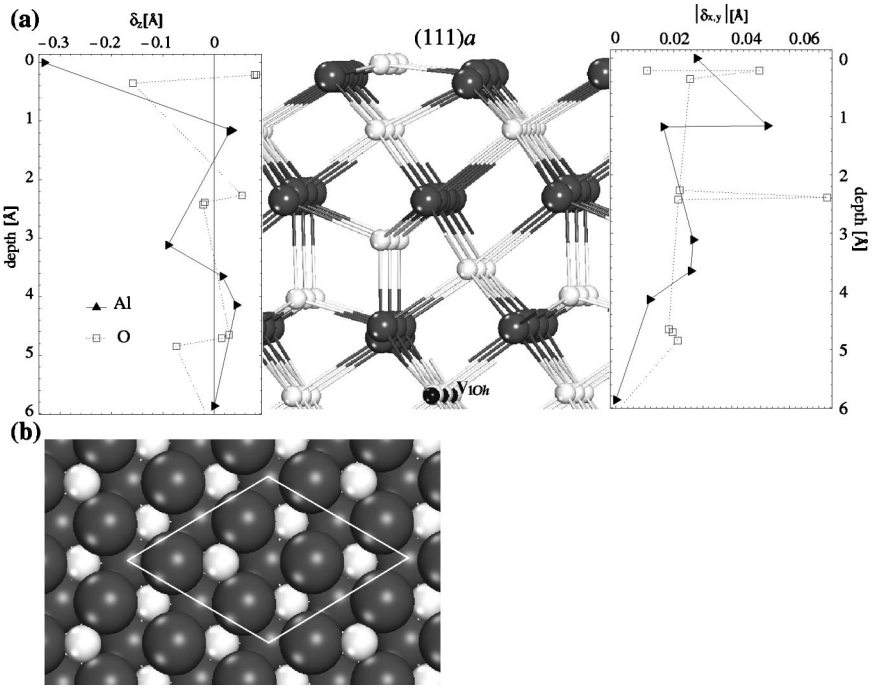

FIG. 7. Outcome of ionic relaxations for the (1 1 1)a surface of γ-Al_2O_3. (a) Left and right panels: ionic displacements normal to the surface (δ_z) and parallel to surface ($|\delta_{x,y}|$) as function of depth within the slab. The positive (negative) values of δ_z mean outward (inward) displacement of the layers with respect to the middle of the slab. The filled triangles and the boxes represent Al and O, respectively. The marks are joined for ease of visualization. (a) Center panel: Atomic structure of the (1 1 1)a surface viewed along [1 1 0]; the white, gray, and black balls denote the Al, O, and vacancy sites, respectively. Notice the position of the V_{O_h}. (b) Top view of this surface.

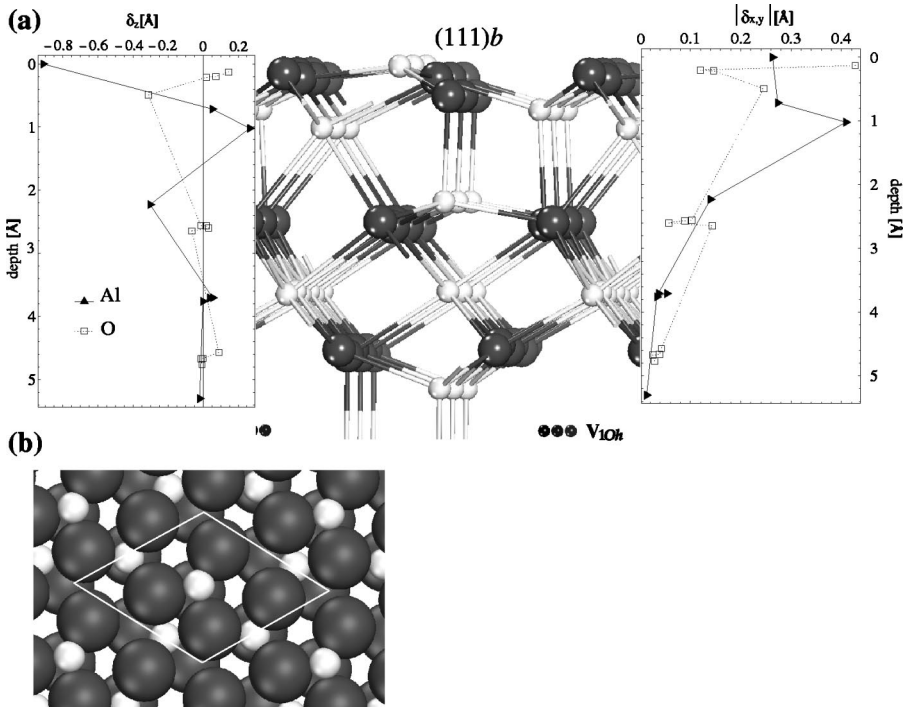

FIG. 8. Outcome of ionic relaxations for the (1 1 1)*b* surface. (a) Ionic displacements as a function of depth within the slab, left and right panels; and its structure in the center panel. (b) Top view of this surface. The marks and colors are the same as in Fig. 7.

0.84 Å and the final is 0.12 Å, giving an M-O_3 change of −0.72 Å or −86%. If we apply the same analysis to all the layers in the slab, we finally find: −86, +4, −42, +21, and +6% for the first five layers M-O_3, O_3-M, M-M, M-O_3, and O_3-M, respectively. This result is in good agreement with previous theoretical and experimental results.[7,9] We note that shifting the topmost Al to other, less symmetrical surface sites results in reconstruction and a >2 J/m^2 increase in σ.

C. Structure of the (1 1 1) surface

The (1 1 1)*a* surface (Fig. 7) has a $M^{T_d}O_4$ termination where the surface metal atoms are threefold coordinated [see Fig. 7(b)], with a layer ordering of $M^{T_d}O_4/M_3^{O_h}/O_4/M^{T_d}/M^{O_h}/M^{T_d}/O_4/M_2^{O_h}$. The outermost Al atoms present a normal inward relaxation (δ_z) with respect to their perfect sites of −0.3 Å with a small planar deformation ($|\delta_{x,y}|$) of 0.03 Å [Fig. 7(a)]. The four O atoms of the outermost close-packed layer (at ~0.05 Å deep) relax normal to the surface, rumpling by ~0.2 Å, so that there is little in-plane distortion ($|\delta_{x,y}|<0.05$ Å). The relaxed surface Al is near trigonal and shows a coverage of 5.95 μmol/m^2. In general, in the (1 1 1)*a* slab, the δ_z and $|\delta_{x,y}|$ relaxations of both Al and O atoms decrease to less than 0.07 Å when the atoms are more than 4 Å deep within the slab. From the left-hand panel of Fig. 7(a) the interlayer relaxation with respect to the bulk spacings were: −58, +4, +0.9, −74, and −5% for the M^{T_d}-O_4, O_4-$M_3^{O_h}$, $M_3^{O_h}$-O_4, O_4-M^{T_d}, M^{T_d}-M^{O_h}, and M^{O_h}-M^{T_d}, respectively. It is important to mention that within the O_4 layer at 2.25 Å deep, the O atoms are threefold coordinated and show small deformations $|\delta_{x,y}|<0.07$ Å. As Fig. 7(a) shows, the topmost Al is on an axis of threefold rotational symmetry with respect to the O and M^{O_h} sublayers down to ~3.5 Å deep.

At first glance, the (1 1 1)*b* surface appears similar to (1 1 1)*a*: it has a $M^{O_h}O_3$ termination with a layer ordering of $M^{O_h}O_3/OM^{T_d}/M^{O_h}/M^{T_d}O_4/M_3^{O_h}/O_4/M^{T_d}$, as shown in Fig. 8. The topmost Al has relaxed $\delta_z=-0.9$ Å from its octahedral position into an almost trigonal site, flush with surface O, with relatively little sideways deformation ($|\delta_{x,y}|=0.3$ Å). However, the distortion in the subsurface layers is an order of magnitude larger in (1 1 1)*b* than in (1 1 1)*a*. The O's at 0.0 and 0.5 Å deep are twofold coordinated ($|\delta_{x,y}|=0.2$ −0.4 Å); the Al at 1 Å deep is five coordinate ($\delta_z=+0.3, |\delta_{x,y}|=0.4$ Å), and only 2.6 Å from the topmost Al. The interlayer M^{O_h}-O_3, O-M^{T_d}, M^{T_d}-M^{O_h}, M^{O_h}-M^{T_d}, M^{T_d}-O_4, and distances undergo variations of −86, −62, −41, +87, −41, and −1%, respectively. Consistent with these severe distortions, we note that the topmost Al in (1 1 1)*b* does not lie on an axis of symmetry with respect to subsurface Al.

The outcome of the MD simulation for the (1 1 1)*a* surface shows no important structural changes. Analysis reveals MSD in the (1 1 1)*a* slab of 0.025 and 0.023 Å^2 for the superficial Al and O layers, respectively, while for the bulk-like Al and O layers at more than 3.5 Å depth [Fig. 7(a)] the MSD are 0.012 and 0.016 Å^2, respectively.

1. Electronic structure of the (1 1 1) surface

Mulliken analysis was carried out for the most stable γ-Al_2O_3 surface, (1 1 1)*a*. The effective charge and overlap population values exhibit only minor changes compared with the bulk. A direct comparison of the effective charges of the atoms in the first layer with the corresponding atoms in the bulk (Table II) show no significant changes, except for the most superficial Al and the four O belonging to the first layer with $q_{\text{eff}}(\text{surf})-q_{\text{eff}}(\text{bulk})=-0.14\ e$ and 0.04 e, respectively, i.e., there is a slight electron transfer from the three-coordinated Al to the first layer of O. We find no appreciable

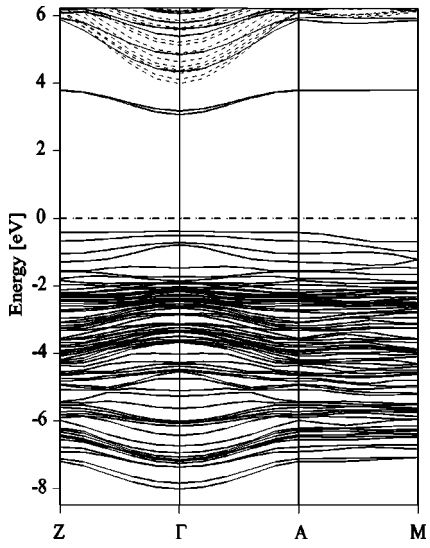

FIG. 9. Calculated (1 1 1)*a* surface band structure of γ-Al_2O_3. The bands in dashed lines are the surface-projected bulk conduction band structure. The zero of energy corresponds to the bulk UVB maximum (dotted-dashed line).

change in the Al-O overlap population within the first layer, meaning that, in spite of the considerable inward relaxation, there is no increase in the covalency of the surface.

We have carried out a GGA calculation of the band structure of the (1 1 1)*a* slab, and this is shown in Fig. 9. Energies were aligned by matching the O semicore *s* states of the lower VBs of slab and bulk. A detailed comparison of the upper VBs showed that no surface states intrude into the bulk band gap (Fig. 4). For this reason, the surface projection of the bulk upper VB is omitted from Fig. 9. For the slab, the states at the top of the upper VB exhibit high electronic localization mainly on the oxygens at 0.2 Å deep. Indeed the electronic density distribution of the highest occupied slab states reveals only small changes with respect to the corresponding state in the bulk, i.e., the electrons remain tightly bound to O atoms, as shown in Fig. 5.

Recognizing that GGA is quantitatively unreliable for excited states, we limit ourselves to qualitative features of the conduction band (CB). The surface-projected bulk CB is drawn in dashed lines in Fig. 9. It is evident that the band gap decreases at the surface (3.39 eV) relative to the bulk, due to a low-lying CB surface state. Analysis reveals that this state is localized on the topmost trigonal Al, similar to the established data on (0 0 0 1) α-Al_2O_3 (Ref. 8). Overall, the reduced dispersion of the surface CB relative to the bulk indicates that excited electrons at the surface will have larger effective mass.

From a direct comparison between the lowest empty surface state of (0 0 0 1) α-alumina and (1 1 1)*a* γ-alumina, 4.8 and 3.4 eV above the Fermi level respectively, we predict *a priori* that surface Al on α-(0 0 0 1) is less reactive than that on γ-(1 1 1)*a*.

D. Structure of the (0 0 1) surface

The (0 0 1) surface undergoes large reconstruction on relaxation (Fig. 10). Returning to our model of bulk γ-Al_2O_3, two types of stoichiometric (0 0 1) layers separated by ~2 Å can be identified: $M_6^{O_h}M_2^{T_d}O_{12}$ and $M_4^{O_h}M_4^{T_d}V_2^{O_h}O_{12}$. Cleaving through the vacancies of the latter yields a 100-atom bulk-terminated slab, which is our starting structure. A feature of this termination is highly undersaturated surface Al [two-coordinate, formerly T_d; Al(1) and Al(2) in Fig. 10(a)]. These

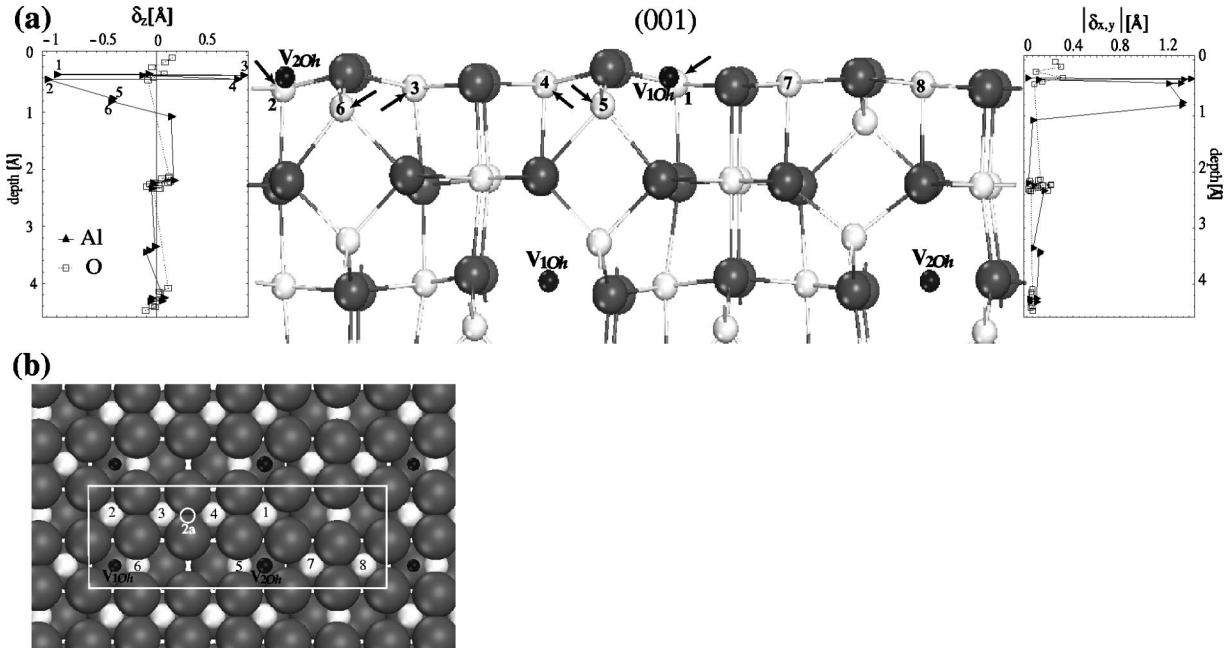

FIG. 10. (a) Outcome of ionic relaxations for the (0 0 1) surface as a function of depth within the slab and a view of its structure. Notice the arrows that show the ionic relaxations and stress the site exchange: Al(4), Al(5) and Al(3), Al(6). (b) Top view of this surface. The numbers in (a) and (b) are in correspondence.

Al atoms are unstable and relax into five-coordinate surface sites. This in turn precipitates a spontaneous O_h-T_d exchange at the surface, with other Al in adjacent (1 1 0) planes relaxing in opposite directions into nonspinel sites [Al(4), Al(5) and Al(3), Al(6) in Fig. 10]. As the figure shows, Al displacements are as much as 1 Å. It is important to note that atoms of the subsurface and central slab layers undergo much smaller displacements, so that we are confident that they remain bulklike.

Edge-linked [0 0 1]-oriented Al_{T_d}-O_2-Al_{T_d} is thus generated just below the surface, showing short Al-Al (2.6–2.7 Å, about 1 Å less than in the bulk). This means that in the adjacent (100) plane a subsurface octahedral vacancy is opened up while the surface V_{O_h} has been eliminated. The three-atom-linked Al displacements [Al(1)-Al(4)-Al(5) and Al(2)-Al(3)-Al(6) in Fig. 10(b)] have thus effected a net V_{O_h} migration of 3.8 Å diagonally away from the surface and *towards* bulk V_{O_h}, giving V_{O_h}-V_{O_h} of just 2.5 Å.

With two such three-atom-linked displacements occurring per unit cell, we observe the generation of one tetrahedral vacancy in the space between. We therefore denote the layers as

$$M_6^{O_h}V^{T_d}/O_{12}/M_2^{T_d}/M^{T_d}/M_6^{Oh}V_2^{O_h}O_{12}/M^{T_d}/M_2^{T_d}/M_4^{O_h}V_2^{O_h}O_{12}/M_2^{T_d}$$

(where the topmost M^{O_h} are in fact five coordinate). Reflecting the migration of V_{O_h} away from the surface, a surface of predominantly five-coordinate Al_{O_h} is favored, at a coverage of 10.44 μmol/m^2. Fully coordinated Al_{T_d} do occur as well [atoms Al(5), Al(6)] and result in rumpling in the Al sublattice of 0.8 Å.

We considered an alternative arrangement of superficial Al_{T_d} as a starting structure [2a in Fig. 10(b)]. A similar pattern of Al exchange was observed on relaxation, to give a surface energy of 1.24 J/m^2 (structure not shown).

The outcome of the MD simulation for the (0 0 1) surface shows no important structural changes. The MSD for the Al and O layers on the surface are 0.018 and 0.020 Å^2, respectively, and for the bulklike Al and O layers at more that 3.3 Å depth [Fig. 10(a)] these values are 0.017 and 0.018 Å^2, respectively.

E. Other surfaces

We have computed two different (1 1 0)-terminated slabs, both 5.6 Å thick (80 atoms for an Al_{O_h}-terminated slab and 100 atoms for a mixture of both Al_{O_h} and Al_{T_d} before relaxation) and observe that both surfaces undergo massive reconstruction into open, amorphous structures. Interestingly, the 80-atom slab, with σ=1.53 J/m^2, displays a sawtooth surface structure (Fig. 11), which we interpret as microfacets along (1 1 1) and (1 1 $\bar{1}$). Al shows fivefold coordination within the (1 1 1) facets and three/four coordination within (1 1 $\bar{1}$). The creation of these small planes after optimization supports the (1 1 1)*a* surface as the most stable bare surface. The 100-atom slab with lower surface energy shows no sawtooth surface and a lower surface energy (σ=1.46 J/m^2 in Table III), consistent with the smaller δ_z displacements than in the 80-atom slab. This result points out the relation between the presence of Al_{O_h} atoms on the surface and its stability. Although not shown in Fig. 11, we found that (1 1 0) has high porosity, perhaps related with the position and orientation of the V_{O_h} vacancy sites.

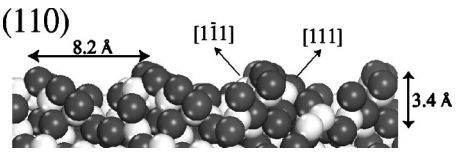

FIG. 11. Side view along [$\bar{1}$ 1 0] of the (1 1 0) surface after a massive relaxation. Note the sawtooth formation with small planes pointing to [1 1 1] and [1 1 $\bar{1}$] directions.

Examination of the (1 $\bar{5}$ 0) superficial atoms after relaxation reveals Al with two-, three-, and fivefold coordination (not illustrated here). The outermost O undergo large deformations $|\delta_{x,y}|$ of 0.88 Å with small δ_z of +0.28 Å; the same behavior is found for the twofold coordinated O at 1.12 Å deep with relaxations $|\delta_{x,y}|$ (δ_z) of 0.83 (+0.032) Å. We observe the largest deformation $|\delta_{x,y}|$=1.2 Å of the Al_{T_d} at 0.7 Å deep, while the remaining Al atoms down to 1.6 Å deep have relaxations of $<$0.38 Å.

V. DISCUSSION

We present an extensive study of stoichiometric γ–alumina surfaces. Three of these are composed of close-packed O: γ-(1 1 1)*a*, α−(0 0 0 1), and γ-(1 1 1)*b* (Figs. 6–8), with surface energies of 0.95, 1.54, and 1.85 J/m^2, respectively. The range of stabilities can be rationalized by looking at the Al sublattice and its effect on the O layers. The topmost Al lies in all cases over a subsurface cation vacancy and so relaxes into an almost trigonal site within the O layer, lowering the surface dipole moment. In this respect, our results agree with many other calculations, where Al-Al interactions are found to govern the relaxation of undercoordinated Al.[8,28,30] No other Al atoms show substantial displacements. If the coverage of trigonal Al is low and if the trigonal Al is symmetrical with respect to subsurface Al, then this relaxation can be accommodated with minimum distortion of the O layer, giving a stable surface, such as γ-(1 1 1)*a*. The interaction between trigonal Al and a disordered arrangement of cations beneath the surface is destabilizing, as is the case in γ-(1 1 1)*b*.

The computed electronic structure shows that bonding at the (1 1 1) surface is similar to that in bulk γ-Al_2O_3 (Sec. III), where we find that Al_{T_d} is bound slightly more covalently than Al_{O_h}. A low-lying CB state is localized on the trigonal Al of (1 1 1), a consequence of its coordinative undersaturation and mobility in *z*, which means that the trigonal Al behaves as a strong Lewis acid and as the adsorption site for electron-rich molecules.

Simply to preserve stoichiometry, the surface Al coverage decreases from α−(0 0 0 1) to γ-(1 1 1), consistent with the lower density of reactive sites on the latter,[48] and the surface is stabilized as the coverage decreases. Extrapolating this trend to more disordered transition aluminas, we expect that

they will show an even lower density of surface Al above close-packed O, and a correspondingly lower surface energy. However, this must be offset by the energetic penalty of deformations in subsurface Al and O, which we predict should accompany a disordered Al sublattice [as calculated for γ-(1 1 1)*b*]. A low density of trigonal Al within (1 1 1) surfaces may explain the lack of three-coordinate Al measured by NMR.[24]

The (0 0 1) surface is computed to behave differently to (1 1 1). The loose, square arrangement of O anions permits considerable flexibility in the surface Al, most of which relax into neighboring nonspinel sites (Sec. IV D) and octahedral vacancies are repelled from the (0 0 1) surface into the slab interior, as in Ref. 27. However, by calculating a larger slab than Ref. 27 (in *x* as well as *z*), we find that surface reconstruction can occur without destruction of the slab, and we are able to identify the barrierless three-atom-linked exchange mechanism that displaces V_{O_h} towards the bulk. This facile motion and undercoordination means that both five-coordinated and tetrahedral Al are moderate Lewis acids.

However, we are aware that the pattern of Al_{O_h}, Al_{T_d}, and V_{T_d} which we obtain is not correlated with the subsurface structure, and is probably an arbitrary product of our choice of cell. Other arrangements atop the cubic substrate would probably be isoenergetic, as long as the 6:2 ratio of five-coordinate Al to Al_{T_d} is preserved. Our finding of Al_{T_d} close to the surface is supported by solid-state NMR of γ-Al_2O_3 (Ref. 24) and by FT-IR,[23] although NMR indicates a slightly higher proportion of ($\sim$6:3).

From the MSD values for MD simulations of (1 1 1)*a* and (0 0 1) surfaces, one can estimate the root-mean-square displacements (RMSD) that, for a simple harmonic oscillator, are related to its vibrational amplitude. We thus obtain amplitudes for the atoms at the surface in the (1 1 1)*a* and (0 0 1) slabs of 1.3 and 1.05 times larger than those in the bulk, respectively. Considering the close similarity in structure of (1 1 1)*a* γ-alumina and (0 0 0 1) α-alumina, our approximate value of 1.3 is in accordance with the value of 1.5 founded previously for (0 0 0 1) α-alumina.[51]

We find that the (1 1 0) and (1 5 0) polar terminations are unstable. The relaxed (1 1 0) surface is rough, with O_h vacancy sites remaining at the surface, and when there are no Al_{O_h} atoms on the unrelaxed slab, the surface reconstructs by microfaceting into (1 1 1)-related segments. This is at odds with the results of Ref. 28, which are based on a hydrogen spinel in a thinner slab with frozen atoms. Our study is far from exhaustive however, and we recognize that other more stable (1 1 0) surfaces may exist.

The (0 0 1) and (1 1 1)*a* surfaces are found to be equally stable, with surface energies that differ by just 0.1 J/m^2, which is close to the limit of computational accuracy. These are purely thermodynamic considerations: the kinetics of various methods of alumina preparation (e.g., dehydration of boehmite, oxidation of metal) may favor other surfaces. Because of their metastability and microporosity, it is hard to prepare well-defined γ-Al_2O_3 surfaces under controlled conditions. A few such measurements are reported and indicate that (0 0 1) and (1 1 0) occur on γ-Al_2O_3.[1,52] Atomistic simulation predicts the energetic ordering (0 0 1)$<$(1 1 1)$<$(1 1 0) in γ-Al_2O_3[50] and (0 0 1)$<$(1 1 0)$\approx$(1 1 1) for $MgAl_2O_4$ spinel.[53] It is encouraging therefore that support for the (0 0 1) surface comes from a wide variety of methods; on the other hand, further work will be necessary to resolve whether (1 1 0) or (1 1 1) also occurs.

Differences are reported in the surface reactivity of η and γ transition aluminas.[28] To a first approximation, we expect the surface chemical reactivity to be governed by its electronic structure (incorporating surface connectivity and coverage). Based on their surface band gaps, we thus predict a higher chemical reactivity of the γ-(1 1 1)*a* and (0 0 1) surfaces relative to α-Al_2O_3 (0 0 0 1). However the Lewis acidity is a macroscopic quantity which depends on both the electron structure and the coverage of active sites. Therefore, it is important to note that γ-(0 0 1) shows a much higher concentration of less acidic five-coordinate Al (10.44 $\mu mol/m^2$) than is the case for the more reactive three-coordinate Al of γ-(1 1 1)*a* (5.95 $\mu mol/m^2$). Obviously, in real surfaces, the temperature, together with surface defects, will change our predictions to some degree.

Finally, except for (1 1 1)*a* γ-Al_2O_3, all the γ-alumina surfaces studied here present considerable instability (large $|\delta_{x,y}|$), behavior already seen in other alumina surface studies.[30] Certainly, the presence of both Al_{Td} and vacancies on the surface are responsible for such instability and the resulting surface structures.

VI. CONCLUSION

Density-functional theory has been applied to the quantitative elucidation of structure and energetics of low index surfaces of transition aluminas. Surface energies of 1.00 ± 0.05 J/m^2 were computed for both (1 1 1) and (0 0 1) surfaces of the γ-Al_2O_3 crystal, and so we conclude that either surface could occur. It follows that γ-Al_2O_3 films are thermodynamically stable with respect to α-Al_2O_3 up to a thickness of about 9 Å. Some less stable surfaces reconstruct so as to produce (1 1 1) microfacets. (1 1 1) surfaces are computed to be mostly O terminated, with a low coverage of trigonal Al behaving as a strong Lewis acid. The (0 0 1) surface is highly reconstructed to give Al in nonspinel sites; it is dominated by five-coordinate Al, with some tetrahedral Al, both of which are expected to be weaker Lewis acids. Given the high-level theoretical treatment and good agreement with experiment, these models may reliably represent a range of transition alumina surfaces.

ACKNOWLEDGMENTS

This research was supported by the European Community under the "Information Society Technologies" program through the HIKE project (http://www.nmrc.ie/hike) and by the Academy of Finland through its Centers of Excellence Program (2000–2005). We acknowledge generous grants of computing time from the NMRC Photonics Theory Group and from the Center for the Scientific Computing (CSC), in Espoo, Finland.

*Also at Centro de Investigación en Física de la Materia Condensada, Corporación de Física Fundamental y Aplicada, Apartado 17-12-637, Quito, Ecuador. Electronic address: henry.pinto@nmrc.ie
†Electronic address: Risto.Nieminen@hut.fi
‡Electronic address: simon.elliott@nmrc.ie

[1] I. Levin and D. Brandon, J. Am. Ceram. Soc. **81**, 1995 (1998).
[2] M. Leskelä and M. Ritala, Thin Solid Films **409**, 138 (2002).
[3] A. Paranjpe, S. Gopinath, T. Omstead, and R. Bubber, J. Electrochem. Soc. **148**, G465 (2001).
[4] D. Ha, D. Shin, G. H. Koh, J. Lee, S. Lee, Y. S. Ahn, H. Jeong, T. Chung, and K. Kim, IEEE Trans. Electron Devices **47**, 1499 (2000).
[5] E. P. Gusev, M. Copel, E. Cartier, I. J. R. Baumvol, C. Krug, and M. A. Gribelyuk, Appl. Phys. Lett. **76**, 176 (2000).
[6] R. DiFelice and J. E. Northrup, Phys. Rev. B **60**, R16 287 (1999).
[7] X.-G. Wang, A. Chaka, and M. Scheffler, Phys. Rev. Lett. **84**, 3650 (2000).
[8] I. Batyrev, A. Alavi, and M. W. Finnis, Faraday Discuss. **114**, 33 (1999).
[9] I. Manassidis and M. J. Gillan, J. Am. Ceram. Soc. **77**, 335 (1994).
[10] E. A. Soares, M. A. VanHove, C. F. Walters, and K. F. McCarty, Phys. Rev. B **65**, 195405 (2002).
[11] C. Wolverton and K. C. Hass, Phys. Rev. B **63**, 024102 (2000).
[12] F. H. Streitz and J. W. Mintmire, Phys. Rev. B **60**, 773 (1999).
[13] R. S. Zhou and R. L. Snyder, Acta Crystallogr., Sect. B: Struct. Sci. **47**, 617 (1991).
[14] G. Gutiérrez and B. Johansson, Phys. Rev. B **65**, 104202 (2002).
[15] E. A. Kotomin and A. I. Popov, Nucl. Instrum. Methods Phys. Res. B **141**, 1 (1998).
[16] J. Carrasco, J. R. B. Gomes, and F. Illas, Phys. Rev. B **69**, 064116 (2004).
[17] E. M. Fernández, L. C. Balbás, G. Borstel, and J. M. Soler, Thin Solid Films **428**, 206 (2003).
[18] G. Renaud, B. Villette, I. Vilfan, and A. Bourret, Phys. Rev. Lett. **73**, 1825 (1994).
[19] G. Gutiérrez, A. Taga, and B. Johansson, Phys. Rev. B **65**, 012101 (2001).
[20] S.-D. Mo, Y.-N. Xu, and W.-Y. Ching, J. Am. Ceram. Soc. **77**, 1193 (1994).
[21] X. Krokidis, P. Raybaud, A. Gobichon, B. Rebours, P. Euzen, and H. Toulhoat, J. Phys. Chem. B **105**, 5121 (2001).
[22] M.-H. Lee, C.-F. Cheng, V. Heine, and J. Klinowski, Chem. Phys. Lett. **265**, 673 (1997).
[23] X. Liu and R. E. Truitt, J. Am. Chem. Soc. **119**, 9856 (1997).
[24] D. Coster, A. L. Blumenfeld, and J. J. Fripiat, J. Phys. Chem. **98**, 6201 (1994).
[25] M. Wilson, M. Exner, Y.-M. Huang, and M. W. Finnis, Phys. Rev. B **54**, 15 683 (1996).
[26] A. Ionescu, A. Allouche, J.-P. Aycard, M. Rajzmann, and F. Hutschka, J. Phys. Chem. B **106**, 9359 (2002).
[27] A. Vijay, G. Mills, and H. Metiu, J. Chem. Phys. **117**, 4509 (2002).
[28] K. Sohlberg, S. J. Pennycook, and S. T. Pantelides, J. Am. Chem. Soc. **121**, 10999 (1999).
[29] O. Maresca, A. Ionescu, A. Allouche, J. P. Aycard, M. Rajzmann, and F. Hutschka, J. Mol. Struct.: THEOCHEM **620**, 119 (2003).
[30] C. Ruberto, Y. Yourdshahyan, and B. I. Lundqvist, Phys. Rev. Lett. **88**, 226101 (2002).
[31] G. Kresse and J. Furthmüller, Comput. Mater. Sci. **6**, 15 (1996).
[32] G. Kresse and J. Furthmüller, Phys. Rev. B **54**, 11 169 (1996).
[33] D. Vanderbilt, Phys. Rev. B **41**, 7892 (1990).
[34] G. Kresse and J. Hafner, J. Phys.: Condens. Matter **6**, 8245 (1994).
[35] J. P. Perdew, J. A. Chevary, S. H. Vosko, K. A. Jackson, M. R. Pederson, D. J. Singh, and C. Fiolhais, Phys. Rev. B **46**, 6671 (1992).
[36] H. J. Monkhorst and J. D. Pack, Phys. Rev. B **13**, 5188 (1976).
[37] V. Milman, B. Winkler, J. A. White, C. J. Pickard, M. C. Payne, E. V. Akhmatskaya, and R. H. Nobes, Int. J. Quantum Chem. **77**, 895 (2000).
[38] R. S. Mulliken, J. Chem. Phys. **23**, 1833 (1955).
[39] D. Sánchez-Portal, E. Artacho, and J. M. Soler, Solid State Commun. **95**, 685 (1996).
[40] D. Sánchez-Portal, E. Artacho, and J. M. Soler, J. Phys.: Condens. Matter **8**, 3859 (1995).
[41] T. Yokokawa and O. J. Kleppa, J. Phys. Chem. **68**, 3246 (1964).
[42] Y. Yourdshahyan, U. Engberg, L. Bengtsson, B. I. Lundqvist, and B. Hammer, Phys. Rev. B **55**, 8721 (1997).
[43] C. Sousa, F. Illas, and G. Pacchioni, J. Chem. Phys. **99**, 6818 (1993).
[44] R. H. French, J. Am. Ceram. Soc. **73**, 477 (1990).
[45] J. C. Boettger, Phys. Rev. B **49**, 16 798 (1994).
[46] V. Fiorentini and M. Methfessel, J. Phys.: Condens. Matter **8**, 6525 (1996).
[47] J. Gay, J. Smith, R. Richter, F. Arlinghaus, and R. Wagoner, J. Vac. Sci. Technol. A **2**, 931 (1983).
[48] J. M. McHale, A. Auroux, A. J. Perrotta, and A. Navrotsky, Science **277**, 788 (1997).
[49] J. M. McHale, A. Navrotsky, and A. J. Perrotta, J. Phys. Chem. B **101**, 603 (1997).
[50] S. Blonski and S. H. Garofalini, Surf. Sci. **295**, 263 (1993).
[51] A. Marmier and M. W. Finnis, J. Phys.: Condens. Matter **14**, 7797 (2002).
[52] P. D. Nellist and S. J. Pennycook, Science **274**, 413 (1996).
[53] C. M. Fang, S. C. Parker, and G. de With, J. Am. Ceram. Soc. **83**, 2082 (2000).